Journal of Visualized Experiments

Transpupillary two-photon in vivo imaging of the mouse retina

--Manuscript Draft--

Article Type:	Invited Methods Article - JoVE Produced Video
Manuscript Number:	JoVE61970R1
Full Title:	Transpupillary two-photon in vivo imaging of the mouse retina
Corresponding Author:	Philip Raymond Williams, PhD Washington University in Saint Louis St. Louis, Missouri UNITED STATES
Corresponding Author's Institution:	Washington University in Saint Louis
Corresponding Author E-Mail:	prwillia@wustl.edu
Order of Authors:	Zelun Wang
	Sean McCracken
	Philip Raymond Williams, PhD
Additional Information:	
Question	**Response**
Please specify the section of the submitted manuscript.	Neuroscience
Please indicate whether this article will be Standard Access or Open Access.	Open Access (US$4,200)
Please indicate the **city, state/province, and country** where this article will be **filmed**. Please do not use abbreviations.	St Louis, Missouri, United States of America
Please confirm that you have read and agree to the terms and conditions of the author license agreement that applies below:	I agree to the Author License Agreement
Please provide any comments to the journal here.	

TITLE:

Transpupillary Two-photon In Vivo Imaging of the Mouse Retina

AUTHORS AND AFFILIATIONS:

Zelun Wang[1,2], Sean McCracken[1,2], Philip R. Williams[1,3,4]

[1]John F. Hardesty, MD Department of Ophthalmology and Visual Sciences at Washington University School of Medicine in St. Louis, St. Louis, Missouri 63110
[2]Graduate Program in Neuroscience at Washington University School of Medicine in St. Louis, St. Louis, Missouri 63110
[3]Department of Neuroscience at Washington University School of Medicine in St. Louis, St. Louis, Missouri 63110
[4]Hope Center for Neurological Disorders at Washington University School of Medicine in St. Louis, St. Louis, Missouri 63110

zelun.wang@wustl.edu
smccracken@wustl.edu

Corresponding author: Philip R. Williams, prwillia@wustl.edu

KEYWORDS:

retina, *in vivo* imaging, two-photon microscopy, retinal ganglion cells, amacrine cells, microglia

SUMMARY:

In vivo imaging is a powerful tool for the study of biology in health and disease. This protocol describes transpupillary imaging of the mouse retina with a standard two-photon microscope. It also demonstrates different in vivo imaging methods to fluorescently label multiple cellular cohorts of the retina.

ABSTRACT:

The retina transforms light signals from the environment into electrical signals that are propagated to the brain. Diseases of the retina are prevalent and cause visual impairment and blindness. Understanding how such diseases progress is critical to formulating new treatments. In vivo microscopy in animal models of disease is a powerful tool for understanding neurodegeneration and has led to important progress towards treatments of conditions ranging from Alzheimer's disease to stroke. Given that the retina is the only central nervous system structure inherently accessible by optical approaches, it naturally lends itself towards in vivo

imaging. However, the native optics of the lens and cornea present some challenges for effective imaging access.

This protocol outlines methods for in vivo two-photon imaging of cellular cohorts and structures in the mouse retina at cellular resolution, applicable for both acute- and chronic-duration imaging experiments. It presents examples of retinal ganglion cell (RGC), amacrine cell, microglial, and vascular imaging using a suite of labeling techniques including adeno-associated virus (AAV) vectors, transgenic mice, and inorganic dyes. Importantly, these techniques extend to all cell types of the retina, and suggested methods for accessing other cellular populations of interest are described. Also detailed are example strategies for manual image postprocessing for display and quantification. These techniques are directly applicable to studies of retinal function in health and disease.

INTRODUCTION:

In vivo visualization of the central nervous system generally requires invasive procedures like skull thinning and installation of glass windows or optical relay lenses. The retina is the only structure in the nervous system that can be directly observed without the need for invasive preparation as it natively receives light from the environment. The ease of optical access to the retina makes it an attractive model system for studying the central nervous system.

Live fluorescent imaging of the retina in mice has been used to track RGC death in models of glaucoma[1,2], optic nerve injury[1,3,4], and stroke[5], as well as changes in microglial activation[6-8] and vasculature[9] in degenerative conditions. Intrinsic signals can also be used to visualize photoreceptors[10-12] and retinal pigment epithelial cells[13]. Many approaches to in vivo imaging of the retina use either highly specialized devices specifically designed for ophthalmological purposes[6] or highly modified optical systems to correct for the native aberrations of the cornea and lens[8,9,11-14].

The present protocol demonstrates an approach to in vivo imaging of fluorescent signals in the retina at cellular resolution, utilizing a basic method of partially correcting for the anterior optics of the mouse eye. This strategy requires very minor adaptations to multiphoton microscope setups that are commonly used for in vivo imaging of the brain. As this approach is straightforward to set up, and the mice are under little stress, it is conducive to perform time-lapse experiments over both acute and chronic durations. Additionally, genetic and organic dye-based procedures that label individual retinal components, including RGCs, amacrine cells, microglia, and vasculature, are compatible with this imaging technique and enable in vivo observation of cell types and structures critical for retinal function. These tools can be adapted to label most other neuronal cell types as well as glial and vascular components of the retina.

PROTOCOL:

NOTE: The following procedure was performed in compliance with the guidelines of the Institutional Animal Care and Use Committee at Washington University in St. Louis. See the **Table of Materials** for details about the reagents, equipment, and animals used in this study.

1. Adeno-associated virus injection

NOTE: Labeling of specific cells in the retina can be accomplished in Cre transgenic mouse lines with restricted patterns of expression. This section describes intravitreal delivery of AAV-associated vectors that encode Cre-dependent expression of a fluorescent protein, thus labeling specific retinal cells. Inject mice (male and female), starting at 4 weeks of age.

1.1. Preparing the micropipette needle

1.1.1. Use a micropipette puller to create a borosilicate glass capillary needle. Load a glass capillary in the micropipette puller and perform the Ramp Test, recording the resulting value. Discard the glass capillary used for the Ramp Test.

1.1.2. Pull micropipettes with the following settings: heat: Ramp Test value minus 10; pull: 55; velocity: 65; time: 120; air pressure: 500; air time at start of pull: 20.

NOTE**:** Settings may need to be adjusted for different pullers.

1.1.3. Under a dissecting microscope, use a razor blade to cut the tip of the pulled micropipette at the location where the glass tip deflects slightly under force, ~10 mm from the end of the tapered section. Cut at a sharp angle such that the cut produces a beveled tip. Discard blunt tips.

1.2. Preparing injection syringe

1.2.1. Fit a cut glass micropipette into a 2 cm segment of ethyl vinyl acetate (EVA) plastic tubing (0.05" inner diameter, 0.09" outer diameter). Connect the other end of this tubing segment to a 20 cm length of EVA tubing (0.02" inner diameter, 0.06" outer diameter).

1.2.2. Connect the tubing to a 50 μL glass syringe with a 22 G cemented needle. Remove the plunger from the glass syringe and backfill the syringe and connected tubing with mineral oil using a 25 G syringe needle. Leave 4 mm air space at the tip of the micropipette.

1.3. Intravitreal injection of AAV

1.3.1. Perform intravitreal injection with standard aseptic technique, using sterile surgical gloves, clean lab coat, mask, sterile field, and autoclaved instruments according to institutional protocols for survival surgery.

1.3.2. Remove an aliquot of AAV vector from storage at -80 °C and thaw on ice. After thawing, centrifuge for 10 s at 2,000 × *g* to remove any air bubbles.

1.3.3. Follow the anesthesia and controlled substances guidelines of the institutional Animal Studies Committee. Using a 30 G hypodermic needle, perform a 0.1 mL/10 g body weight intraperitoneal (IP) injection of a ketamine/xylazine cocktail (10 mg/mL ketamine, 1 mg/mL xylazine in saline, effective dose to mouse: 100 mg/kg ketamine, 10 mg/kg xylazine). Return the mouse to its cage and allow 5 min for anesthesia to take effect.

1.3.4. Using a 30 G hypodermic needle, perform a 0.1 mL/10 g body weight subcutaneous injection of meloxicam (0.5 mg/mL in 0.9% sodium chloride).

1.3.5. Test the depth of anesthesia by confirming loss of corneal reflex and withdrawal reflex to tail and toe pinch. If corneal reflex persists after loss of tail and toe withdrawal reflex, apply a drop of 0.5% proparacaine solution to each eye and wait for 10 s.

1.3.6. Place the mouse on its side under the stereomicroscope. Use a mini bulldog hemostatic clamp to grab the skin superior and inferior to the orbit, and secure the clamp at the medial canthus to partially displace the globe up out of the orbit.

1.3.7. Puncture the lateral sclera with the cut micropipette connected to the glass syringe, ~1–2 mm posterior to the limbus. Avoid disturbing the vasculature that runs circumferentially immediately posterior to the limbus. Perform the puncture at an angle perpendicular to the sclera, and slightly retract the micropipette immediately after piercing the sclera to avoid damaging the lens.

1.3.8. Use the plunger of the glass syringe to withdraw 1–2 μL of vitreous humor, corresponding roughly to the fluid volume intended for injection. Withdraw the micropipette from the eye, and eject the removed vitreous humor.

1.3.9. Fill the tip of the micropipette with 1–2 μL of AAV, leaving ~4 mm of air space between the viral vector and the mineral oil to avoid mixing. Insert the micropipette in the hole in the sclera created by the first puncture, and slowly press the plunger of the glass syringe to inject the viral vector over the course of 20–30 s. Visualize the fluid level of the viral vector in the tip of the micropipette, and be careful to stop injecting before any air enters the eye.

1.3.10. Hold the micropipette in the same position for 10 s, then retract the micropipette. Remove the bulldog hemostatic clamp.

1.3.11. Apply oxytetracycline/polymyxin B antibiotic ophthalmic ointment to the injected eye. Place the mouse on a heating pad, and monitor its recovery from anesthesia (see 3.4.3).

1.3.12. Return the mouse to its housing, and perform postoperative care per institutional guidelines. Allow 2–3 weeks for viral-mediated expression of fluorophores before imaging.

2. Microscope setup

NOTE: A schematic of the microscope light path is shown in **Figure 1**.

2.1. "Always-On" equipment: These instruments should always remain on unless undergoing adjustment or maintenance. Set the high temperature of the laser cooling system to 20.0 °C. Turn on the main power to the ultrafast Ti:Sapphire laser, allow time for completion of system startup processes, and turn the "Laser Enable" key to the "On" position.

2.2. Emission light path configuration

2.2.1. Configure the fluorescence emission collection path to sample wavelengths using appropriate dichroic and band pass filter sets for the fluorophores of interest.

NOTE: In this manuscript, Twitch2b imaging used a filter cube consisting of a 505 long pass dichroic and 480/40 and 535/30 band pass filter pairs. GFP was imaged using a red/green filter cube consisting of a 560 long pass filter with 525/50 and 605/70 band pass filters. Evans Blue was imaged using a 560 short pass filter. Changing emission filters exposes the emission light path to stray room light that could damage photomultiplier tubes (PMTs). Ensure PMTs are turned off, and turn off room lights prior to modifying the collection light path as light exposure can adversely affect PMT function.

2.3. Starting up image acquisition

NOTE: Direct exposure to the two-photon laser is hazardous, especially to the eye as far-red light will not induce a blink response. Proper care should be taken to ensure that the laser is closed along the light path, and fail-safes are in place to protect the user from exposure via the eye pieces or emissions from the microscope objective. Users should understand under which conditions the laser will emit from the objective, and take proper precautions not to expose themselves to such hazards.

2.3.1. Turn on the data acquisition device, computer, Pockels cell, microscope and stage controller, mechanical shutter controller, and PMT main power. Keep PMTs in the "Disabled" state until ready for image acquisition and shielded from stray light. Open the laser control interface on the computer and image acquisition software. Turn on the laser from the computer interface and ensure mode-locking.

2.3.2. Set the desired laser wavelength. Ensure that laser light is entering the Pockels Cell by opening the laser shutter, and allow 30 min for laser power to stabilize.

2.4. Measuring laser power at the objective and setting maximum laser percentage

NOTE: Laser radiation emits from the objective lens during power measurement. Close the microscope enclosure curtain, and wear appropriate eye protection prior to enabling the imaging shutter. Measure laser power at the time of initial system installation to establish the power

output curve for each wavelength of interest and monthly thereafter to verify the stability of excitation power.

2.4.1. Turn on the optical power meter, and select the measurement wavelength corresponding to the laser wavelength. Place the optical power meter detector on the microscope stage and maneuver it directly under the objective lens in the X-Y dimensions. Using the Z-dimension motorized focus drive, lower the objective lens until the power meter detector is ~1 mm below the objective lens.

2.4.2. Switch from epifluorescence illumination to the laser as the microscope excitation light path. Enable the mechanical shutter.

2.4.3. In the image acquisition software, start a point scan to open the imaging shutter, and send the laser to the optical power meter. Set the laser power to 100% in the scanning software. Optimize the X-Y and Z positions of the power meter detector until at a location giving the highest laser power measurement.

2.4.4. Measure laser power at the objective from 0.1% to 100% on the Pockels Cell, taking measurements at 10% intervals. Record the Pockels Cell percentage corresponding to 45 mW of power at the objective. Set this percentage as the maximum laser power in the image acquisition software.

NOTE: The highest power observed for in vivo mouse retinal imaging without visible damage to the target tissue was 45 mW, as assayed by histological staining two weeks after imaging. Obvious retinal damage is evident after imaging with 55 mW at the objective.

2.4.5. Disable the imaging shutter and return the excitation light path to epifluorescence.

3. Preparation of mouse for image acquisition

3.1. Anesthetizing mouse for imaging

NOTE: Ensure proper waste gas scavenging to mitigate exposure to isoflurane. Make sure the exhaust port of the anesthesia induction chamber is connected to a passive scavenging gas filter cannister, and the outlet of the mouse anesthesia nosepiece is connected to an active scavenging gas filter cannister with vacuum provided by a gas evacuation apparatus. Follow the manufacturer's guidelines for monitoring the filter canister weight for replacement.

3.1.1. Anesthetize the mouse using the ketamine/xylazine cocktail as described above in step 1.3.3. Alternatively, induce anesthesia via isoflurane inhalation if also using isoflurane for maintenance of anesthesia (imaging session > 30 min). Set the small animal anesthesia device to fill the induction chamber with 5% isoflurane mixed with room air at a flow rate of 0.5 L/min. Place the mouse in the induction chamber, and allow 15 s for the mouse to become anesthetized.

3.1.2. Switch the isoflurane vaporizer to 0%, and direct the anesthesia flow to the nosepiece. Perform a 5-s "O_2 flush" of the induction chamber. Take the mouse out of the induction chamber, and secure it in the head holder (see section 3.3), attaching the nosepiece.

3.1.3. Use a mixture of 1% isoflurane with room air at a flow rate of 0.5 L/min for maintenance of anesthesia. Monitor respiratory rate at 5-minute intervals throughout anesthesia, adjusting the isoflurane percentage to maintain a respiratory rate of ~60 breaths/min.

NOTE: These settings (% isoflurane, flow rate) can also be used for maintenance of anesthesia induced by the ketamine/xylazine cocktail.

3.2. Pupil dilation

3.2.1. Prepare a solution of 1% w/v atropine and 2.5% w/v phenylephrine hydrochloride in water. Store the dilator solution at room temperature protected from light.

3.2.2. Using a disposable pipette eye dropper, apply a drop of the dilator solution to each eye that will be imaged. Turn off the room lights, and wait 5 min for the pupil to dilate. When the pupil is dilated, blot away the dilator solution with lint-free tissue.

NOTE: Ensure dilator solution does not enter the nostrils.

3.2.3. Apply a large drop of lubricant eye gel to each eye that will be imaged. If both eyes are to be imaged, apply a small piece of plastic cling film over the eye gel on the non-imaging eye to prevent dehydration. If only imaging one eye, apply lubricant eye ointment to the eye that will not be imaged.

3.3. Positioning mouse for imaging

3.3.1. To secure the mouse in the imaging head holder, rotate the main arm of the head holder until the earpiece bar is tilted at an angle of 60° or more below horizontal. Secure the lower ear canal pin in the inward extended position and the upper ear canal pin in the withdrawn position.

3.3.2. With the mouse facing the bite bar, mount one ear onto the extended lower pin, inserting the pin into the ear canal. Loosen the screw securing the upper ear canal pin, and extend the pin into the other ear canal. Tighten the screw to secure the head.

3.3.3. Slide the bite bar toward the head of the mouse. Gently elevate the head of the mouse, then lower the maxillary incisors of the mouse into the hole of the bite bar. Retract the bite bar with gentle force to secure the head of the mouse, and secure the bite bar position by tightening the screw.

3.3.4. If using isoflurane, slide the nosepiece through its slot onto the bite bar prior to securing the incisors of the mouse. Secure and tighten the bite bar position as in step 3.3.3. Tighten the

nosepiece using the two screws on its upper face until it fits snugly on the nose of the mouse, but does not constrict the snout.

3.3.5. Transfer the mouse, in the head holder, to the microscope stage beneath the objective. Rotate the main arm of the head holder until the pupil of the eye is oriented straight up in line with the light path (**Figure 2**).

3.3.6. Place a #1.5 coverslip in the compact filter holder, and attach the holder to the microscope stage. Lower the coverslip toward the eye, contacting the lubricant eye gel, such that the coverslip lies horizontally immediately above the cornea (**Figure 2**). Ensure that the coverslip does not touch the cornea.

NOTE: On the microscope, ensure the excitation light path is set to epifluorescence and emission light path is set to eyepiece. Turn on the epifluorescence illuminator at its lowest power and open the illuminator shutter. Choose the epifluorescence illuminator wavelength and fluorescence filter corresponding to the fluorophore being imaged.

3.3.7. Maneuver the stage in the X-Y dimensions and objective in the Z-position using the stage control and motorized focus drive until the widefield excitation light fully covers the cornea. Looking through the eyepiece, continue to adjust the Z-position of the stage until the fluorescent cells or structures in the retina come into focus. Increase epifluorescence illuminator power if the sample signal is insufficiently bright to resolve individual cells or structures of interest through the eyepiece.

NOTE: If having trouble locating the retina, the iris is a good landmark to anchor to and then focus down toward the retina. This step will also allow verification that the pupil is maximally dilated.

3.3.8. Obtain an imaging area on axis with the mouse lens. Adjust the angle of the mouse using the various degrees of freedom on the head holder until only expansion or contraction of out-of-focus light occurs when adjusting the focal plane. Turn off the epifluorescence illuminator and close the illuminator shutter.

NOTE: Significant X-Y parallax of out-of-focus light while scrolling through the Z-direction focal planes indicates that the retina is not on axis with respect to the imaging light path.

3.4. Two-photon image acquisition

3.4.1. Image setup and acquisition parameters

NOTE: Turn off room lights, and cover stray light sources in the room. Ensure the epifluorescence illuminator is off, and the illuminator shutter is closed.

3.4.1.1. Switch the excitation light path to the laser and emission light path to the PMTs.

3.4.1.2. In the image acquisition software, set a frame size of 512 x 512 and frame average of 3. Set the steps per slice to -8 µm. Designate z-stepping to start at the top of the stack and progress downward, minimizing two-photon laser activation of photoreceptors.

NOTE: The step size can be reduced to increase Z-resolution at a cost of increased imaging time, but 8 µm steps are sufficient to resolve cell somata in this imaging configuration.

3.4.1.3. Turn on and enable the PMTs. Adjust the PMT voltage to 680 V. Enable the imaging and emission shutters.

NOTE: Powered PMTs are susceptible to light damage. Ensure that the epifluorescence illuminator is off, the microscope enclosure curtain is drawn, and room lights are off.

3.4.1.4. Begin a live image preview of the target tissue, starting with 1% laser power. Auto adjust the display brightness to visualize the cells or structures of interest. Auto adjust the scan phase. If the target tissue is dim or unclear, increase the laser power percentage until structures become visible without surpassing the limit set in step 2.4.4 corresponding to 45 mW.

NOTE: For a 16-bit image, a display value of ~1000 when auto adjusting brightness in a Z-plane containing structures of interest indicates sufficient brightness of the sample.

3.4.1.5. Maneuver the microscope stage in the X-Y direction to center on a desired imaging area, then navigate to the Z-plane with the structures of interest in focus.

NOTE: Imaging adjacent to the optic nerve head allows it to serve as an unambiguous landmark for chronic imaging experiments.

3.4.1.6. If this is a chronic time-lapse experiment, have a previous image open on the acquisition computer, and use it as a reference to find the same area of interest. Ensure that the angle of imaging is similar to that of previous images to acquire the same set of cells with minimal parallax.

NOTE: Further adjustment of the mouse head position is likely required to image the same cells as in previous time points (**Figure 3**).

3.4.1.7. Set the Z-limits of the imaging stack by navigating to the uppermost and lowermost Z-planes of interest, and acquire the image. Upon completion of image acquisition, disable the PMTs and the laser shutter. Switch the emission light path back to the eyepiece, and the excitation light path to epifluorescence illumination. Remove the mouse from the microscope stage.

3.4.2. System software and hardware shutdown

3.4.2.1. Exit the image acquisition software. Turn off the laser in the computer interface. Shut down hardware in reverse startup order, with the exception of the "Always-On" Equipment.

3.4.3. Mouse recovery

3.4.3.1. Remove the head holder and mouse from the microscope stage. If applicable, set the isoflurane vaporizer to 0%. Remove the mouse from the head holder.

3.4.3.2. Gently wipe off lubricant eye gel with a lint-free tissue, and apply white petrolatum-mineral oil lubricant eye ointment to both eyes. Place the mouse on the warm water circulating heating pad (set at 37 °C), continue attending to the mouse and monitoring its respiratory rate until the mouse wakes up and regains ambulatory capacity. Return the mouse to its housing.

3.4.3.3. If applicable, assess animal activity and morbidity at 24 h post intravitreal injection Upon completion of study, euthanize the mouse by transcardial perfusion with 4% paraformaldehyde

3.5. Image processing and analysis

3.5.1. Deinterleave and merge multichannel data

3.5.1.1. As certain image acquisition software programs store multichannel images in an interleaved format, open the .tif image file using software, such as Fiji (https://imagej.net/Fiji), to separate the channels.

3.5.1.2. In the **Image** menu of Fiji, select **Stacks | Tools | Deinterleave**. Input the number of channels composing the image and click **OK**.

3.5.1.3. To merge the separated channels into a single file, go to **Image | Color | Merge Channels**. Place the deinterleaved image channels into separate color channels, and click **OK** to create the multichannel composite image. Save this composite image as a new .tif file.

3.5.2. Quantification of fluorescence intensity in multichannel images

NOTE: Fluorescence intensity within designated regions of interest (ROIs) can be quantified in single-image planes using Fiji. Quantification of ratiometric readouts can be achieved by measuring the fluorescence intensity in different channels of a composite image within the same ROI. For chronic imaging experiments, it is best to use biosensors based on excitation or emission ratiometric outputs.

3.5.2.1. In Fiji, go to **Analyze | Tools | ROI Manager**. Open the composite image in Fiji. Scroll to the z-slice corresponding to the structure of interest, and use the **Selection tools** (such as Rectangle selection, Oval selection, Polygon selection) to outline the ROIs.

3.5.2.2. Press **T** on the keyboard to add each selection to the ROI Manager. Upon completion of ROI selection, click on **Measure** in the **ROI Manager** to record various data from the ROIs such as **Area** and **Mean Intensity value**. Go to **Analyze | Set Measurements to customize data fields for display**.

3.5.2.3. Copy the measurements for the currently selected channel recorded in the **Results** window to a spreadsheet. Switch to the next **Channel** in the **Composite image** window and click on **Measure** to obtain measurements for that channel within the same set of ROIs. Within the **ROI Manager**, go to **More | Save**, and save the ROIs (as a .zip file, if necessary).

3.5.3. Maximum intensity projections for display

3.5.3.1. To create displays of the image data, use the Z-project function in Fiji. In the **Image** menu, select **Stack | Z project**. Choose only the frames within which areas of interest are present to reduce the background.

3.5.3.2. If removal of PMT shot noise is desired, use the **Median filter function**. In the **Process** menu, select **Process | Filters | Median**. Choose a value of **1.0** to maintain spatial details.

3.5.3.4. To create maximum-intensity projections focused on single cells, repeat this process choosing only the image frames that correspond to the cell of interest.

NOTE: This can greatly improve the ability to resolve cellular arbors (**Figure 4**). Measurements of fluorescence intensity should be performed in single-image planes and not on maximum intensity projections.

REPRESENTATIVE RESULTS:

Various transgenic, viral vector, or inorganic dye-labeling approaches can be used to specifically visualize several retinal cells types and structures in vivo using a simple adaptation of a basic multiphoton microscope. To visualize RGCs and amacrine cells, VGlut2-Cre and VGat-Cre transgenic mice, respectively, were given an intravitreal injection of a Cre-dependent AAV expression construct encoding Twitch2b, a cytoplasmic fluorescence resonance energy transfer (FRET)-based Ca^{2+} sensor that contains cyan and yellow fluorescent proteins (CFP and YFP, respectively) and the Ca^{2+} binding domain of troponin[15]. In VGlut2-Cre mice, RGC somas are clearly discernable, and fascicles of axons are often apparent (**Figure 3**).

It should be noted that the trajectory of axons and the negative image of the vasculature makes it very straightforward to identify the optic nerve head in VGlut2-Cre mice, which is useful as a landmark in chronic imaging experiments (**Figure 3**). Although amacrine cells appear less bright than RGCs, possibly due to their smaller soma size and/or less efficient AAV transduction, their somas are still readily apparent in the inner nuclear layer. In contrast to RGCs, amacrine cell

neurites are more often observed in the inner plexiform layers (**Figure 5**). Retinal microglia can be imaged in the Cx3cr1-GFP transgenic mouse line[6]. Microglia associate with the vasculature, making it possible to find the same region in time-lapse imaging experiments.

This approach can be used to track the dynamics of fine microglia processes, a procedure that has better spatial resolution in single-plane images, or if maximum-intensity projections are prepared focusing on individual cells (**Figure 4**). The poor axial resolution caused by optical aberration through the mouse lens precludes examination of fine details in the z-dimension. To determine whether this imaging technique can observe degenerative changes in cellular ultrastructure, 1 µL of 50 mM *N*-methyl-D-aspartate (NMDA) was injected into the vitreous to induce excitotoxic lesion. One day after injection, the microglia demonstrated short processes or amoeboid morphology (**Figure 4**) in accordance with previous reports[16]. It should be noted that cells in the Cx3cr1-GFP transgenic line exhibited more uniform and complete fluorescent protein expression across the cellular cohort than in experiments with AAV-mediated delivery of fluorescent protein expression cassettes. The benefits of varied and sparse versus complete and uniform labeling should be considered when designing experiments.

To label retinal vasculature as previously described[8], mice were injected intraperitoneally with 200 µL of Evans blue dye (20 mg/mL in sterile saline) 30–60 min before imaging. This led to strong labeling of blood vessels emanating from the optic nerve head (**Figure 6**). Surprisingly, the fluorescent signal of a single injection persisted for at least seven days. Two distinct methods were used to estimate the dimensions of the in vivo images. First, the same retinal regions were imaged in vivo and after fixation in flattened retinal wholemounts using confocal microscopy (**Figure 7**). Random cell pairs were selected from four different in vivo samples, and the true distance between cell pairs was measured in confocal scans and matched with in vivo pixel distance to obtain an average pixel size of 0.99 µm with 1x digital magnification. Using similar methods correlating in vivo images with confocal wholemount scans has revealed that a single head position allows for imaging over a roughly 650 mm^2 patch of retina.

Repositioning of the head holder along one torsional axis can allow access to a linear region of the retina 2.2 mm in length (not shown). Further, 1 or 2 µm diameter fluorescent microspheres were injected into the eyes of mice and their diameter was measured as full-width half-maximum of line scans from in vivo images with 10x digital zoom. This gave a slightly larger pixel size estimate, but with more variance (**Figure 7**). Overall, confocal imaging of wholemount samples after completion of in vivo experiments is the most consistent method to assign scale to individual images, as variance in corneal and lens properties may alter image scale from sample to sample.

FIGURE LEGENDS:

Figure 1: Light path schematic. The basic components of the two-photon microscope used in this protocol consist of a Pockels Cell to modulate laser power, a lens pair to reduce the laser beam diameter to match the back aperture of the microscope objective, and a pair of galvo scan mirrors

for beam steering. A pair of steering mirrors is present before each major optical component. The focus is controlled by a motor that drives the objective mount. The emission light path can be customized for different fluorophores by changing out dichroic and barrier filters. A general setup for cyan/yellow/red imaging is displayed in which a short pass dichroic mirror directs red light to the first PMT, and a long pass dichroic mirror paired with appropriate band pass filters is used to separate cyan and yellow emissions. Abbreviation: PMT = photomultiplier tube.

Figure 2: Positioning mice for in vivo imaging. To position the mouse with the pupil on axis with the light path, the anesthetized mouse is first restrained in a head holder, the head is rotated and angled, a large drop of lubricant eye gel is placed on the eye, and the mouse is placed on the stage. A coverslip is mounted in the coverslip holder perpendicular to the light path and lowered down towards the eye. The coverslip should not contact the cornea or mouse head (left), which will be evident if the coverslip is deflected. However, the coverslip should also be close enough to avoid waisting of the droplet (right), because this will have a demagnifying effect on the sample. After applying the gel immersion and securing the coverslip, the stage should be moved in place directly under the microscope objective.

Figure 3: Imaging retinal ganglion cells. For image display, maximum intensity projections with the z-planes containing cells of interest are created, and resultant images are median-filtered to remove PMT shot noise. Two examples of retinal ganglion cells labelled by injecting AAV-EF1α-FLEX-Twitch2b into VGlut2-Cre transgenic mice are shown, specifically the CFP signal. Images were acquired at sessions four days apart, and vascular landmarks were used to return to the same region near the optic nerve head. The optic nerve head is oriented towards the bottom of the image. Although both samples show some variance in orientation (regions with decreased intensity are indicated with arrows), most cells are present at both time points. Scale bar = approximately 50 µm. Abbreviations: PMT = photomultiplier tube; AAV = adeno-associated virus; EF1α = elongation factor-1alpha; FLEX = flip-excision; VGlut2 = vesicular glutamate transporter 2; CFP = cyan fluorescent protein.

Figure 4: Imaging amacrine cells. Amacrine cells were labeled by injecting AAV-EF1α-FLEX-Twitch2b into VGat-Cre transgenic mice. The CFP signal of Twitch 2b is specifically shown. Small maximum-intensity projections focused on the depths of the inner nuclear layer indicate amacrine cell somas, while focusing on the inner plexiform resolves amacrine cell neurites (arrow). The optic nerve head is oriented towards the right of the image. Scale bar = approximately 50 µm. Abbreviations: AAV = adeno-associated virus; EF1α = elongation factor-1alpha; FLEX = flip-excision; VGat = vesicular gamma aminobutyric acid transporter; CFP = cyan fluorescent protein; INL = inner nuclear layer; IPL = inner plexiform layer.

Figure 5: Imaging microglia. The transgenic mouse line Cx3cr1-GFP was used to label microglia. A maximum-intensity projection of the full scan volume shows many microglia, some with fine process detail that can be resolved. Note that cells towards the lower left of the field have less distortion in the maximum projection than those towards the upper right due to parallax in this region. Maximum-intensity projections containing only the cell of interest significantly reduces this parallax (center, boxed in corresponding colors). Furthermore, this imaging strategy can

document the dynamics of fine microglia process remodeling (lower panels). Comparatively, many microglia can be seen with short processes or amoeboid morphology one day after an excitotoxic lesion by intravitreal injection of 50 mM NMDA (right). Scale bar = approximately 50 µm. Abbreviations: GFP = green fluorescent protein; Cx3cr1 = Cx3 chemokine receptor 1; NMDA = *N*-methyl-D-aspartate.

Figure 6: Labelling vascular landmarks. Mice were injected with 200 µL of 20 mg/mL Evans blue intraperitoneally 30–60 min prior to the first imaging session. Full thickness maximum-intensity projections demonstrate lasting fluorescence in the retinal vasculature that persisted for at least seven days. Scale bar = approximately 50 µm.

Figure 7: Image dimensions. Retinal ganglion cells labelled by injecting AAV-EF1α-FLEX-Twitch2b into VGlut2-Cre transgenic mice were imaged in vivo, and the same region was then imaged by confocal laser scanning microscopy after fixation and wholemount preparation of the retina. Yellow fluorescent protein channel is shown for both. Colored arrow pairs indicate the same cell in both preparations (upper panels). Single-plane image of 2 µm diameter fluorescent microspheres injected intravitreally and imaged in vivo (lower left panel). Microspheres did not settle and thus were in constant motion making measurement of axial resolution impossible. Pixel sizes calculated from full-width half-maximum measurements of in vivo fluorescent microspheres or correlative confocal measurements taken from 2–4 retinas per group (lower right). Scale bar = 50 µm. Abbreviations: AAV = adeno-associated virus; EF1α = elongation factor-1alpha; FLEX = flip-excision; VGlut2 = vesicular glutamate transporter 2.

Figure 8: Calcium activity induced by two-photon scanning. Retinal ganglion cells labelled by injecting AAV-EF1α-FLEX-Twitch2b into VGlut2-Cre transgenic mice, YFP is pseudocolored magenta and CFP green, imaged in a single plane as a time series at 4.22 Hz. All RGCs had a similar starting YFP/CFP ratio. Most responded with an increase in FRET ratio (excluding the orange cell), and one maintained a high YFP/CFP ratio throughout the time series (yellow cell). YFP/CFP ratios were normalized to the first frame average, and colored circles match with colored traces. Scale bar = 20 µm. Abbreviations: AAV = adeno-associated virus; EF1α = elongation factor-1alpha; FLEX = flip-excision; VGlut2 = vesicular glutamate transporter 2; YFP = yellow fluorescent protein; CFP = cyan fluorescent protein; RGCs = retinal ganglion cells; FRET = fluorescence resonance energy transfer.

DISCUSSION:

The anatomy of the eye presents unique challenges to in vivo imaging, as the high optical power of the mouse cornea and lens impedes direct imaging though the pupil without correction. Several other in vivo imaging methods rely on the use of a plano-concave contact lens for correction of the anterior optics of the mouse eye[7,17-19]. The two-photon imaging procedure described herein enables longitudinal in vivo imaging of the mouse retina. Repeatable images of the same region of retina can be obtained for a continuous period of up to 6 or more h under isoflurane. The mouse can also be imaged on different days using cellular and vascular landmarks

to locate the same imaging area (**Figure 3**). The use of a clear gel immersion combined with cover glass for this purpose has previously been applied to a range of procedures, including visualization of retina for subretinal injection, laser-induced retinal injury models, and fundus imaging[20-22].

With only optical correction at the cornea, the high optical power of the mouse lens results in an inevitable amount of parallax, particularly of structures in the peripheral scan field, manifesting as stretching and translational movement in the X-Y dimension at different Z-planes. To minimize image parallax-related distortion in X and Y dimensions, it is crucial that the mouse eye is oriented such that the tangent plane to the retina at the imaging area is perpendicular to the microscope light path. The setup described here is conducive to precise manipulation of the angle of the eye to achieve this alignment. An adjustable mouse head holder that permits rotation along two axes allows for easy manual adjustments of the angle of the eye as the experimenter scrolls through the Z-dimension to minimize parallax. This tilting also circumvents the field stop effect of the pupil to permit imaging greater areas of the retina. The restraint of the head holder also greatly reduces motion artifacts caused by respiration.

Care must be taken to maintain clarity of the mouse eye, as image quality will deteriorate with opacification during continuous imaging. Frequent reapplication of lubricant gel during imaging, and ointment application after each imaging session help to prevent the eye from drying and developing opacities. Some corneal opacities will spontaneously resolve after 24–48 h. The use of clear gel and cover glass as described in this protocol provides for similar image quality and aberration correction as a contact lens[7], while allowing for easier adjustments of the eye angle without the need to realign the cover glass. Additionally, the gel provides continual hydration to the eye, making it possible to perform acute imaging sessions of up to several hours. Finally, since the cover glass does not contact the cornea, it causes minimal irritation to the eye that may reduce optical clarity for repeat imaging sessions.

A limitation of this approach is the fact that optical aberrations are not entirely corrected. While this severely diminishes axial resolution due to the heavy parallax, quantitative measurements of the soma can be obtained in single-image planes. It should be noted that as fluorescence signal intensity of retinal neurons is dependent on sample alignment with this method, excitation and emission ratiometric based sensors are more appropriate for experiments comparing samples chronically across different imaging sessions. An approach to correct optical aberrations at the system level is adaptive optics, which allows for subcellular resolution in the retina[8,9,14,21]. However, adaptive optics requires highly specialized equipment and extensive expertise to implement.

Alternative approaches to two-photon in vivo retinal imaging are confocal microscopy or ophthalmoscopy[6]. The approach presented here should be readily translatable to widefield of confocal microscopy. Single photon imaging is perhaps more robust and poses less risk of damaging the retina due to high energy of the two-photon laser necessary to achieve efficient two-photon effect through the cornea and lens of the eye. To avoid two-photon laser damage, the threshold for maximal laser power should be empirically determined by examining

wholemount retinas after completion of imaging experiments and immunostaining for cell types in the layers imaged. In the system presented here, RGCs were labelled with the pan-RGC marker, Rbpms, and densities were normal up to 45 mW imaging power, whereas 55 mW caused a significant loss of RGCs (not shown).

A drawback of single-photon imaging is the fact that this approach will very heavily stimulate the native visual circuits of the retina compared to two-photon imaging[23]. Previous experiments using retinal wholemounts or eyecup preparations have shown that two-photon laser scanning elicits circuit activation that is largely transient[24]. Here, imaging of RGC activity with the Ca^{2+} sensor Twitch2b shows that the onset of laser scanning induces Ca^{2+} elevations, which return to baseline over the course of 5–20 s in most RGCs (**Figure 8**). Given that the laser power in this protocol is in the range of previous experiments reporting in vivo retinal light response[8], the currently described method is likely amenable to recordings of circuit activity in the retina. Such considerations are important for experiments that may be influenced by circuit activity.

This protocol demonstrates in vivo imaging of two types of retinal neurons, RGCs and amacrine cells. Similar labeling of other major cell types can be achieved, including horizontal cells (Cx57-Cre[25]), bipolar cells (Chx10-Cre[26]; mGluR6-GFP[27]), cone photoreceptors (S- or M-opsin-Cre[28]), rod photoreceptors (Nrl-Cre[29]), Müller glia (Foxg1-Cre[26]), and pericytes (NG2-DsRed[9]). Transgenic mice are also available to label discrete subsets of RGCs (e.g., KCNG4-Cre for αRGCs[30]; OPN4-Cre for ipRGCs[31]; JAM-B-CreER for J-RGCs[32]) and amacrine cells (e.g., ChAT-Cre for starburst amacrine cells[26] and neuropeptide promoter drivers for various amacrine cell subtypes [3,34]). Viral vectors can be used to target specific cell populations in lieu of transgenic mice. Intravitreal injections of AAV2 with a ubiquitous CAG promoter element almost exclusively label RGCs, amacrine cells and horizontal cells[25]. Pairing the modified AAV2.7m8-Y444F capsid with an engineered mGluR6 promoter construct allows for broad labeling of ON bipolar cells[35]. Subretinal injections of AAV lead to an enrichment of photoreceptors, with serotype AAV2/5 having the highest transduction efficiency[36]. Shh10, a modified AAV6 capsid protein, paired with glial fibrillary acidic protein promoter elements has been demonstrated specific for Müller glia[37].

The ability to observe cells in the central nervous system with a completely non-invasive approach can be used to study both basic properties of neural circuits[8], as well as mechanisms of neurodegeneration[3-6,38]. Many blinding diseases target cellular populations in the retina, and in vivo imaging approaches in mice have been used to study optic nerve injury[1,3,4], macular degeneration[13], stroke[5], glaucoma[2,6], and uveitis[7]. Furthermore, many central nervous system neurodegenerative conditions manifest in the retina including Alzheimer's disease[39], multiple sclerosis[40], and Parkinson's disease[41]. Therefore, this readily accessible technique for in vivo imaging of the retina can be applied as a tool to study a broad set of neurodegenerative conditions.

ACKNOWLEDGEMENTS:

This work was supported by grants from the Research to Prevent Blindness Foundation (Career Development Award to P.R.W. and an unrestricted grant to the Department of Ophthalmology and Visual Sciences at Washington University School of Medicine in St. Louis), National Glaucoma Research (a program of BrightFocus Foundation), and the McDonnell Center for Cellular and Molecular Neurobiology. Z.W. is supported by an Institutional National Research Service Award T32 EY013360. This work was also supported by the Hope Center Viral Vectors Core at Washington University School of Medicine.

DISCLOSURES:

The authors have nothing to disclose.

REFERENCES:

1 Smith, C. A., Chauhan, B. C. In vivo imaging of adeno-associated viral vector labelled retinal ganglion cells. *Scientific Reports.* **8** (1), 1490 (2018).

2 Liu, H., Ding, C. Establishment of an experimental glaucoma animal model: A comparison of microbead injection with or without hydroxypropyl methylcellulose. *Experimental and Therapeutic Medicine.* **14** (3), 1953–1960 (2017).

3 Chauhan, B. C. et al. Longitudinal in vivo imaging of retinal ganglion cells and retinal thickness changes following optic nerve injury in mice. *PLoS One.* **7** (6), e40352 (2012).

4 Leung, C. K. et al. Longitudinal profile of retinal ganglion cell damage after optic nerve crush with blue-light confocal scanning laser ophthalmoscopy. *Investigative Ophthalmology & Visual Science.* **49** (11), 4898–4902 (2008).

5 Murata, H. et al. Imaging mouse retinal ganglion cells and their loss in vivo by a fundus camera in the normal and ischemia-reperfusion model. *Investigative Ophthalmology & Visual Science.* **49** (12), 5546–5552 (2008).

6 Bosco, A., Romero, C. O., Ambati, B. K., Vetter, M. L. In vivo dynamics of retinal microglial activation during neurodegeneration: confocal ophthalmoscopic imaging and cell morphometry in mouse glaucoma. *Journal of Visualized Experiments.* (99), e52731 (2015).

7 Bremer, D. et al. Longitudinal Intravital Imaging of the Retina Reveals Long-term Dynamics of Immune Infiltration and Its Effects on the Glial Network in Experimental Autoimmune Uveoretinitis, without Evident Signs of Neuronal Dysfunction in the Ganglion Cell Layer. *Frontiers in Immunology.* **7**, 642 (2016).

8 Qin, Z. et al. Adaptive optics two-photon microscopy enables near-diffraction-limited and functional retinal imaging in vivo. *Light: Science & Applications.* **9**, 79 (2020).

9 Schallek, J., Geng, Y., Nguyen, H., Williams, D. R. Morphology and topography of retinal pericytes in the living mouse retina using in vivo adaptive optics imaging and ex vivo characterization. *Investigative Ophthalmology & Visual Science.* **54** (13), 8237–8250 (2013).

10 Williams, D. R. Imaging single cells in the living retina. *Vision Research.* **51** (13), 1379–1396 (2011).

11 Carroll, J., Neitz, M., Hofer, H., Neitz, J., Williams, D. R. Functional photoreceptor loss revealed with adaptive optics: an alternate cause of color blindness. *Proceedings of the National Academy of Sciences of the United States of America.* **101** (22), 8461–8466 (2004).
12 Rossi, E. A. et al. Imaging retinal mosaics in the living eye. *Eye.* **25** (3), 301–308 (2011).
13 Rossi, E. A. et al. In vivo imaging of retinal pigment epithelium cells in age related macular degeneration. *Biomedical Optics Express.* **4** (11), 2527–2539 (2013).
14 Geng, Y. et al. Adaptive optics retinal imaging in the living mouse eye. *Biomedical Optics Express.* **3** (4), 715–734 (2012).
15 Thestrup, T. et al. Optimized ratiometric calcium sensors for functional in vivo imaging of neurons and T lymphocytes. *Nature Methods.* **11** (2), 175–182 (2014).
16 Takeda, A. et al. Microglia mediate non-cell-autonomous cell death of retinal ganglion cells. *Glia.* **66** (11), 2366–2384 (2018).
17 Ikeda, W., Nakatani, T., Uemura, A. Cataract-preventing contact lens for in vivo imaging of mouse retina. *Biotechniques.* **65** (2), 101–104 (2018).
18 Palczewska, G., Kern, T. S., Palczewski, K. Noninvasive two-photon microscopy imaging of mouse retina and retinal pigment epithelium. in *Retinal Degeneration. Methods in Molecular Biology.* Weber, B. H. F., Langmann, T. (Eds), Humana, New York, NY, USA, **1834,** 333–343, doi:10.1007/978-1-4939-8669-9_21 (2019).
19 Wahl, D. J., Jian, Y., Bonora, S., Zawadzki, R. J., Sarunic, M. V. Wavefront sensorless adaptive optics fluorescence biomicroscope for in vivo retinal imaging in mice. *Biomedical Optics Express.* **7** (1), 1–12 (2016).
20 Park, S. W., Kim, J. H., Park, W. J., Kim, J. H. Limbal approach-subretinal injection of viral vectors for gene therapy in mice retinal pigment epithelium. *Journal of Visualized Experiments.* (102), e53030 (2015).
21 Biss, D. P. et al. In vivo fluorescent imaging of the mouse retina using adaptive optics. *Optics Letters.* **32** (6), 659–661 (2007).
22 Shah, R. S., Soetikno, B. T., Lajko, M., Fawzi, A. A. A mouse model for laser-induced choroidal neovascularization. *Journal of Visualized Experiments.* (106), e53502 (2015).
23 Palczewska, G. et al. Human infrared vision is triggered by two-photon chromophore isomerization. *Proceedings of the National Academy of Sciences of the United States of America.* **111** (50), E5445–5454 (2014).
24 Euler, T. et al. Eyecup scope--optical recordings of light stimulus-evoked fluorescence signals in the retina. *Pflügers Archive-European Journal of Physiology.* **457** (6), 1393–1414 (2009).
25 Zhang, Y. et al. Elevating Growth Factor Responsiveness and Axon Regeneration by Modulating Presynaptic Inputs. *Neuron.* **103** (1), 39–51 e35 (2019).
26 Ivanova, E., Hwang, G. S., Pan, Z. H. Characterization of transgenic mouse lines expressing Cre recombinase in the retina. *Neuroscience.* **165** (1), 233–243 (2010).
27 Morgan, J. L., Dhingra, A., Vardi, N., Wong, R. O. Axons and dendrites originate from neuroepithelial-like processes of retinal bipolar cells. *Nature Neuroscience.* **9** (1), 85–92 (2006).
28 Akimoto, M. et al. Transgenic mice expressing Cre-recombinase specifically in M- or S-cone photoreceptors. *Investigative Ophthalmology & Visual Science.* **45** (1), 42–47 (2004).
29 Brightman, D. S., Razafsky, D., Potter, C., Hodzic, D., Chen, S. Nrl-Cre transgenic mouse mediates loxP recombination in developing rod photoreceptors. *Genesis.* **54** (3), 129–135 (2016).

30 Duan, X. et al. Subtype-specific regeneration of retinal ganglion cells following axotomy: effects of osteopontin and mTOR signaling. *Neuron.* **85** (6), 1244–1256 (2015).
31 Ecker, J. L. et al. Melanopsin-expressing retinal ganglion-cell photoreceptors: cellular diversity and role in pattern vision. *Neuron.* **67** (1), 49–60 (2010).
32 Kim, I. J., Zhang, Y., Yamagata, M., Meister, M., Sanes, J. R. Molecular identification of a retinal cell type that responds to upward motion. *Nature.* **452** (7186), 478–482 (2008).
33 Akrouh, A., Kerschensteiner, D. Morphology and function of three VIP-expressing amacrine cell types in the mouse retina. *Journal of Neurophysiology.* **114** (4), 2431–2438 (2015).
34 Zhu, Y., Xu, J., Hauswirth, W. W., DeVries, S. H. Genetically targeted binary labeling of retinal neurons. *Journal of Neuroscience.* **34** (23), 7845–7861 (2014).
35 Lu, Q. et al. AAV-mediated transduction and targeting of retinal bipolar cells with improved mGluR6 promoters in rodents and primates. *Gene Therapy.* **23** (8–9), 680–689 (2016).
36 Surace, E. M., Auricchio, A. Versatility of AAV vectors for retinal gene transfer. *Vision Research.* **48** (3), 353–359 (2008).
37 Yao, K. et al. Wnt regulates proliferation and neurogenic potential of Muller glial cells via a Lin28/let-7 miRNA-dependent pathway in adult mammalian retinas. *Cell Reports.* **17** (1), 165–178 (2016).
38 Williams, P. R. et al. A recoverable state of axon injury persists for hours after spinal cord contusion in vivo. *Nature Communications.* **5**, 5683 (2014).
39 Cheung, C. Y. et al. Microvascular network alterations in the retina of patients with Alzheimer's disease. *Alzheimer's & Dementia.* **10** (2), 135–142 (2014).
40 Kerrison, J. B., Flynn, T., Green, W. R. Retinal pathologic changes in multiple sclerosis. *Retina.* **14** (5), 445–451 (1994).
41 Sung, M. S. et al. Inner retinal thinning as a biomarker for cognitive impairment in de novo Parkinson's disease. *Scientific Reports.* **9** (1), 11832 (2019).

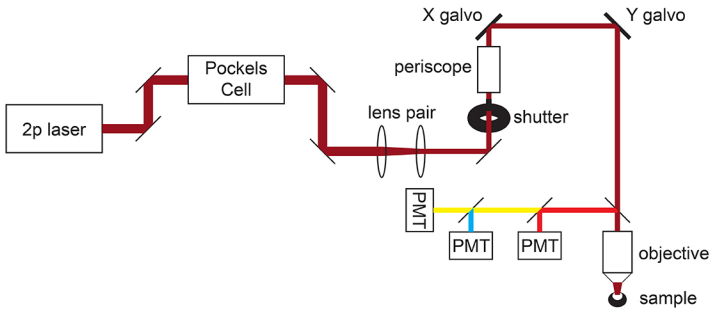

Align pupil and apply eye gel

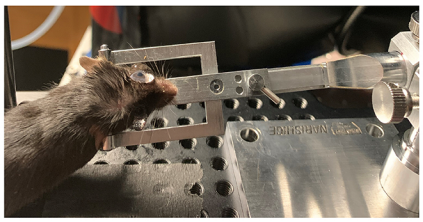

Position coverslip contacting the eye gel but not the eye

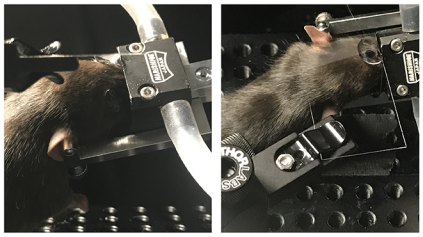

Incorrect coverslip positions:

Coverslip contacting eye Droplet waisting

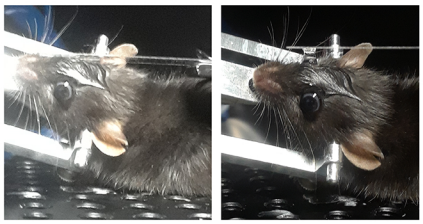

Adjust stage to align pupil with light path

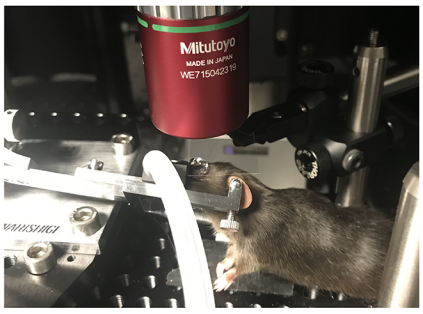

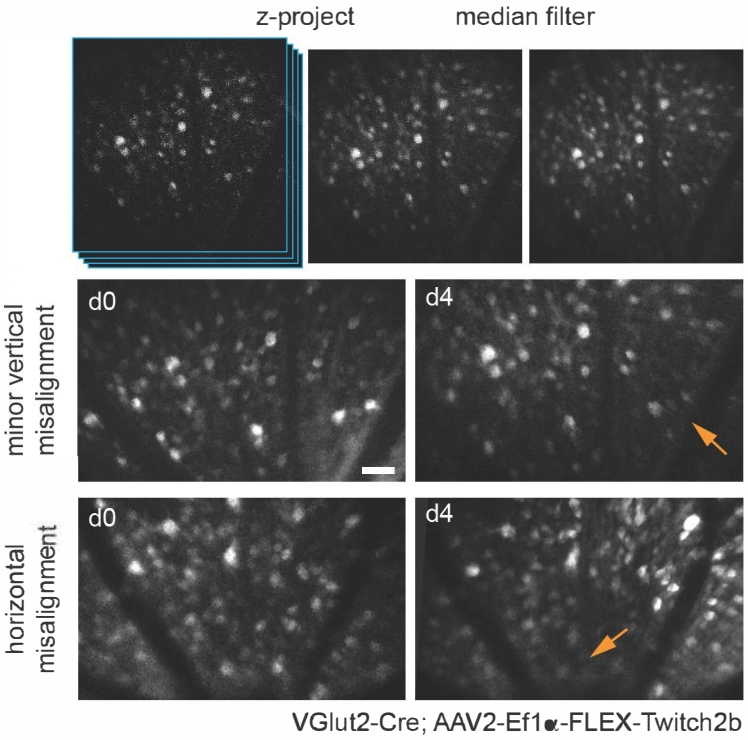

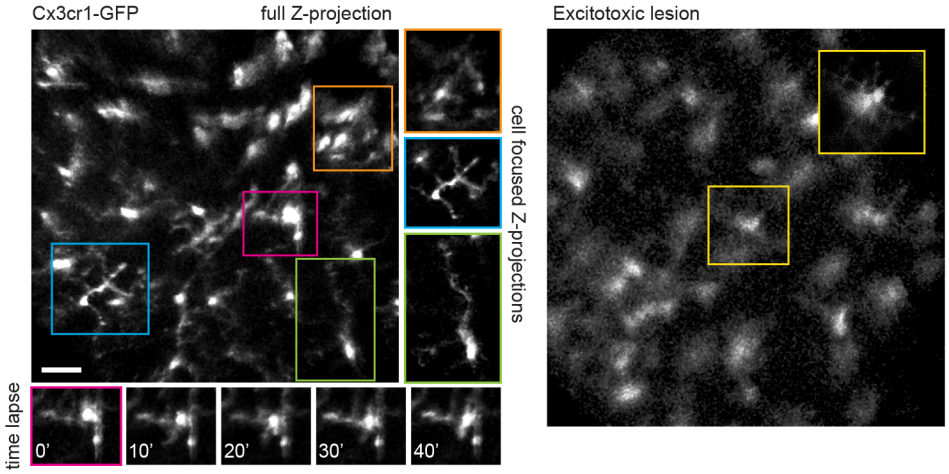

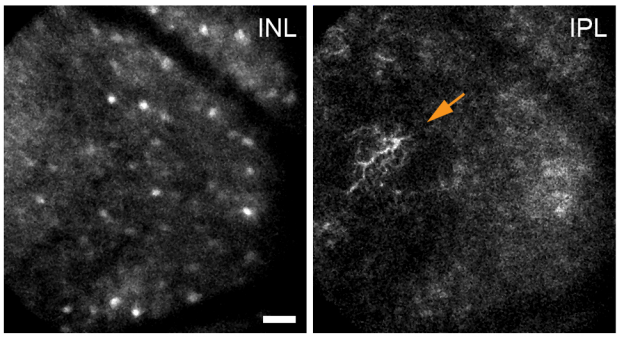

VGat-Cre; AAV2-Ef1α-FLEX-Twitch2b

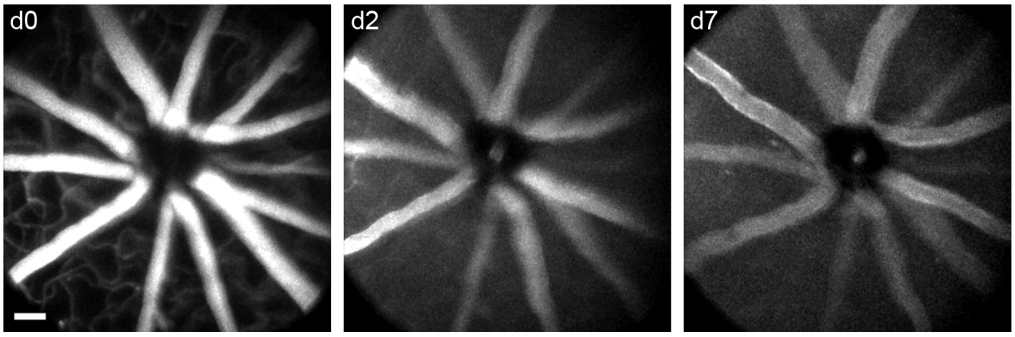

Intraperitoneal Evans Blue

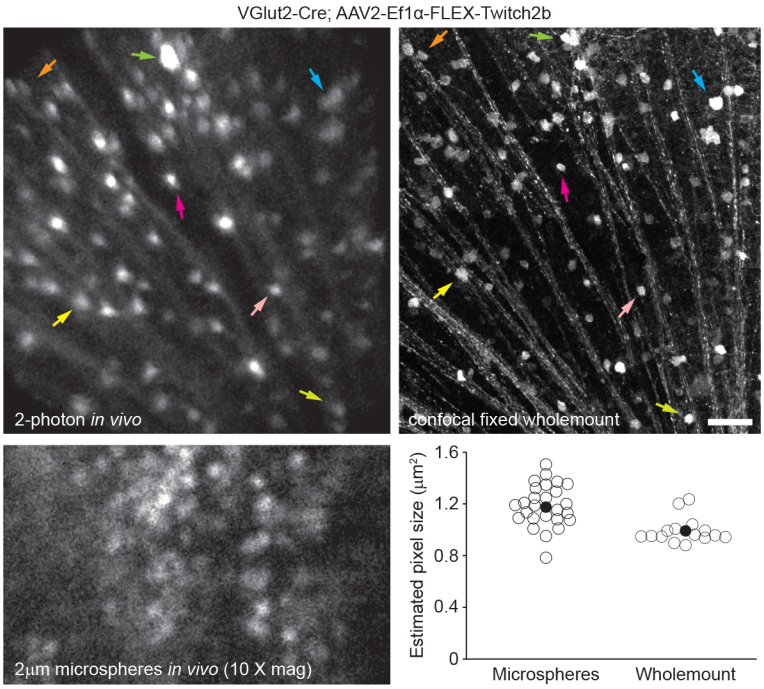

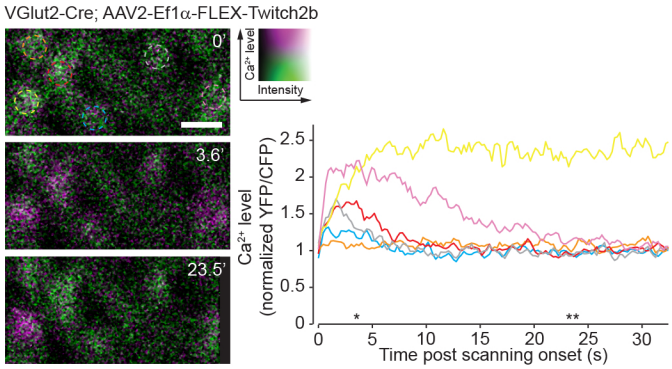

Table of Materials

Click here to access/download;Table of Materials;Wang et al Materials List.xls

Name of Material/ Equipment	Company
#1.5 coverslip	ThermoFisher
50 μL glass syringe	Hamilton
Adeno-associated virus (AAV2)	Hope Center Viral Core
Anesthesia Air Pump	RWD Life Science
Atropine	Sigma
Basic Small Animal Anesthesia Device	RWD Life Science
Borosilicate glass capillary	Sutter
CFP/YFP filter cube	Chroma
ChromoFlex - Two channel PMT detection unit	Scientifica
Circulating heating pump	Braintree Scientific
Cling film	VWR
Compact Filter Holder	ThorLabs
Cx3cr1-GFP transgenic mice (B6.129P2(Cg)-Cx3cr1tm1Litt/J)	The Jackson Laboratory
DAQ controller chassis	National Instruments
Data acquisition device	National Instruments
Evans Blue dye	Fisher Scientific
FPGA module with digitizer	National Instruments
Gas Evacuation Apparatus	RWD Life Science
GenTeal Severe lubricant eye gel	Alcon
GFP/Red filter cube	Chroma
Heating pad	McKesson Medical and Surgical
HyperScope Launch Optics for use with Pockels Cell	Scientifica
HyperScope Main module	Scientifica
HyperScope Scan Path	Scientifica
HyperScope X galvo Module	Scientifica
ImageJ Fiji software	
Isoflurane	Patterson Veterinary
Isoflurane gas filter cannister (active scavenging)	RWD Life Science
Isoflurane gas filter cannister (passive scavenging)	RWD Life Science
ketamine HCl (100 mg/mL)	Vedco
M32 to M26 adapter	ThorLabs
MaiTai GUI software	Spectra-Physics
MATLAB software	MathWorks

meloxicam (5 mg/mL)	Boehringer Ingelheim
Micorscope Objective	Edmund Optics
micropipette puller	Sutter
Mineral oil	Fisher
Mini bulldog hemostatic clamp	Fine Science Tools
Miniature EVA Tubing 0.02" ID, 0.06" OD	McMaster Carr
Miniature EVA Tubing 0.05" ID, 0.09" OD	McMaster Carr
Mouse head holder	Narishige
No. 5 Forceps	Fine Science Tools
Optic Posts 1/2"	ThorLabs
Optical power meter kit	ThorLabs
pE-300 Ultra LLG Deivery	Scientifica
Phenylephrine hydrochloride	Sigma
Pockels cell	Conoptics
Pockels cell amplifier	Conoptics
Proparacaine hydrochloride	Sigma
Red & Far Red short pass filter Cube	Chroma
Rotating 1/2" post clamp	ThorLabs
ScanImage package	Vidrio Technologies
sodium chloride solution, sterile (0.9%)	Fresenius Kabi
Stereomicroscope	Leica
Tabletop centrifuge	Oxford
Terramycin oxytetracycline/polymyxin B antibiotic ophthalmic ointment	Zoetisus
ThermoRack cooling system	Solid State Cooling Systems
Ultrafast Ti:Sapphire laser	Spectra-Physics
Vgat-Cre transgenic mice (Slc32a1tm2(cre)Lowl/J)	The Jackson Laboratory
VGlut2-Cre transgenic mice (Slc17a6tm2(cre)Lowl/J)	The Jackson Laboratory
VivoScope for In Vivo Imaging	Scientifica
White petrolatum-mineral oil lubricant eye ointment	Stye
xylazine HCl (20 mg/mL)	Akorn

Catalog Number		Comments/Description
	152440	Richard-Allan #1.5 24 mm x 40 mm
	80950	22G cemented needle
NA		
R510-30		
A0132		For pupil dilator solution
R500IE		
B150-86-10		Outside diameter 1.50 mm, inside diameter 0.86 mm, length 10 cm
custom		480/40, 505 long pass, 535/30
S-MPLG-1002		
tp-700		Set to 37 °C
10713-916		
DH1		Holds coverslip over mouse eye
005582		
PXIe-1073		
BNC-2090A		
AAA1677409		
NI-5734		
R546W		
(from local pharmacy)		For use during imaging
custom		535/30, 560 long pass, 605/70
	190147	
S-MP-101080		
S-MP-100466		
S-MP-100406		
MP-100443		
Freeware		
NDC 14043-704-06		
R510-31		
R510-31S		
NDC 50989-161-06		
M32M26S		
NA		
NA		R2015b

NDC 0010-6013-01	Analgesic
46-404	Mitutoyo WE715042319
Flaming/Brown Model P-97	
BP2629-1	
18053-28	
1883T1	
1883T4	
SGM-4	
11251-10	
TR3-P5	
PM100D	
COO-LED3ULLGs	
P6126	For pupil dilator solution
350-80-02	
Model 302RM	
1571001	For eye immobilization
custom	560 short pass
SWC	
Freeware	Image acquisition software; Version 5.4.0 (2018); requires MATLAB
NDC 63323-186-01	
S9 E	
Benchmate C8	
NA	For use after intravitreal injection
ThermoRack 401	Set to 20 °C
Mai Tai DeepSee	
016962	
016963	
S-MPVS-1200-00P	
NA	For use after imaging
NDC 59399-110-20	

Reviewer #1:

Manuscript Summary:

The manuscript „Transpupillary multiphoton in vivo imaging of cellular cohorts in the mouse retina" by Zelun Wang and colleagues gives instructions for in vivo two-photon imaging of the mouse retina with a standard multiphoton microscope. The authors use a simple but effective approach to mitigate the optical impact of the mouse cornea. Several examples of applications in transgenic mice with or without additional injections for fluorophore expression in targeted cells/structures are given.

We thank the reviewer for their accurate assessment of our submission.

Major Concerns:

The instructions are clear and straightforward to follow. The simple approach for cancelling the impact of the anterior optics of the mouse eye may be of interest to many research groups. I am wondering whether the authors have ever experienced any problems when scanning across broad areas of the retina. In this case, the beam might be clipped by the animal's pupil when directed to the very extremes of the scan field.

We have measured the range of imaged area in a single head orientation and the data is presented below. We can image an area of roughly 650 μm^2 in a single head orientation. If we tilt the angle of the head across image acquisitions, we can access a linear range of 2.2 mm, and thus estimate an area of the retina across 3.8 mm^2 is accessible for in vivo imaging with our setup. We have added this information to the text.

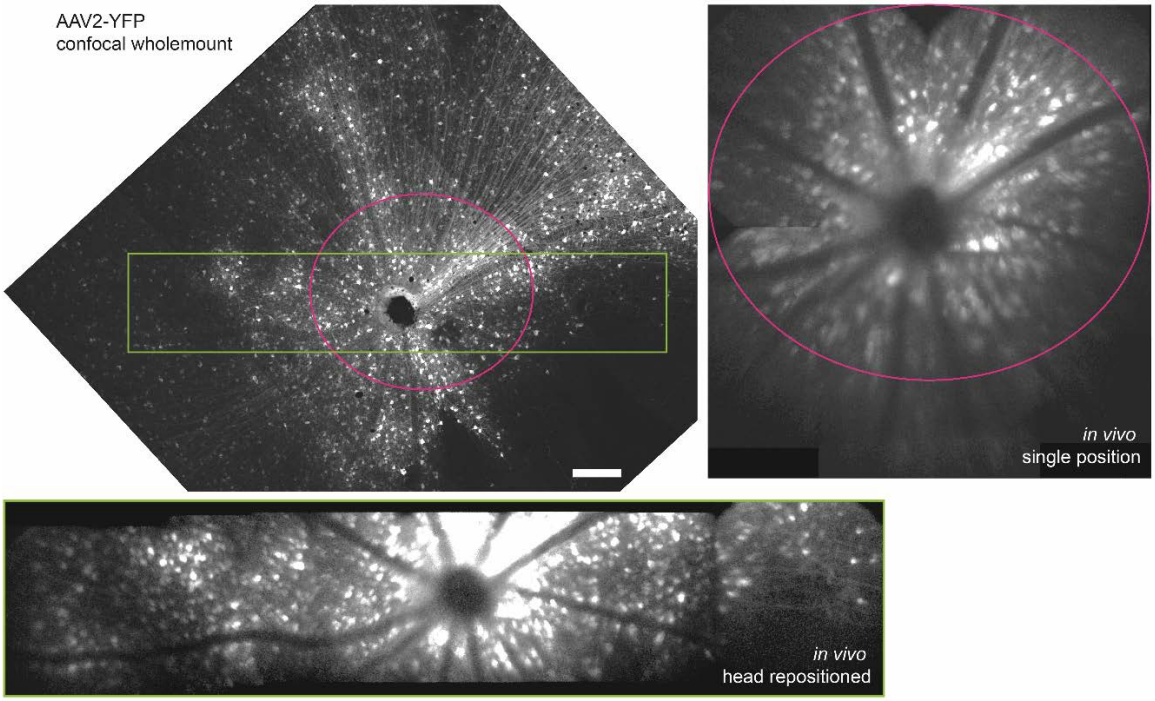

Reviewer Figure 1. Imaging field of view. VGlut2-Cre mouse injected with AAV2-EF1α-FLEX-Twitch2b was imaged *in vivo* and the fixed retinal wholemount was then scanned using confocal microscopy (left, YFP signal displayed). A single head tilt position was imaged *in vivo* across multiple fields of view and stitched (right). Additionally, the mouse's head was tilted to extreme positions around a single point of rotation until the fluorescent signal was lost and stitched

across the center of the retina (bottom). The regions containing RGCs were circled in both the *in vivo* and confocal scans. Scale bar = 200 μm.

A major point for in vivo imaging would be assessment of retinal function. Do the authors believe that their setup is suitable for this purpose? What are the limitations here? Please discuss.

We have investigated calcium responses in retinal ganglion cells (RGCs) in our preparation using the FRET ratiometric sensor Twitch2b. Similar to previous reports from retinal explants, we have found that onset of laser scanning induces a calcium increase in RGCs that returns to baseline in most neurons (see Figure 8). We attempted to add UV LED stimulation to our microscope setup, but unfortunately we were not able to procure the custom mirrors needed to adapt our light path in the time frame for these revisions. However, the 2-photon power that we use for scanning is within the range of previous reports that have observed light responses, and we can clearly observe transient changes in calcium in RGCs. Thus we believe it would be entirely feasible to image circuit activity with our approach. This information has been added to the manuscript.

Minor Concerns:
Apart from the points above, I only have very few comments and suggestions:
Page 5, Line 71: Maintain numbering format: 1) Adeno-associated virus injections (instead of 1.)

These suggestions have been amended in the manuscript.

Page 7, Section 3 and 4: When trouble shooting Maitai start up problems, people should be referred to the Maitai manual.

As suggested, we have removed commercial language from the manuscript.

Page 8, Line 230-234: As far as I understand, the authors did not specifically test for tissue health or light damage. The reported light levels are still very high and far beyond the safety regime. Please rephrase this section more conservatively. Instead of saying "without damage to the target tissue" use for instance the expression "without immediately visible damage to the target tissue" and only state the lowest laser power, for which damage was observed.

We have quantified RGC survival following chronic imaging by immunostaining wholemount retinae for the RGC marker Rbpms. RGC density was not reduced with repetitive imaging of laser powers up to 45 mW at the pupil. However, imaging from 55 mW and up led to severe loss of RGCs. This information has been added to the manuscript and is presented below.

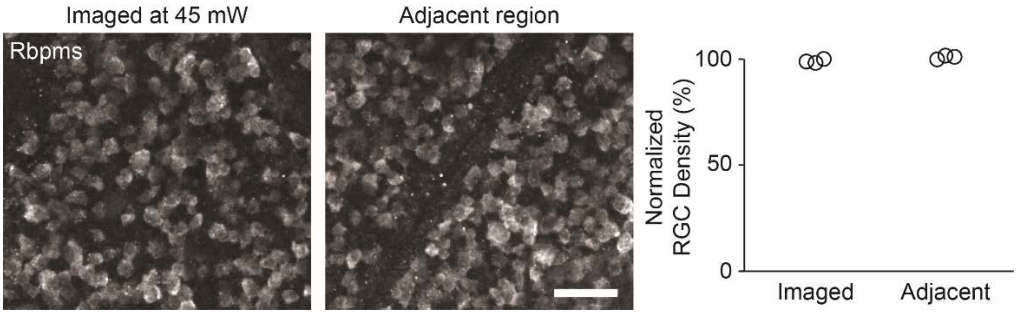

Reviewer Figure 2. RGC survival after repetitive imaging. Confocal scans of Rbpms immunostained retinal wholemounts from an area that was imaged 3 times on different days at

45 mW, and directly adjacent regions. For quantification, RGC densities from imaged and adjacent pairs were averaged and normalized to account for native variance in RGC density across different regions of the retina. Scale bar = 50 μm.

Page 8, line 251: Remove "leaving"
Page 13, line 515: Add "cell types and structures"
Page 15, line 542: Replace "microscope objective" by "light path"
Page 15, line 545: Replace "pupil" by "light path"
Page 15, line 546: Replace "it does" by "the coverslip and the eye gel do"

These suggestions have been amended in the manuscript.

Page 15, line 557: How did the authors calibrate the size of the scan field to obtain the dimension of the scale bar? What is the lateral and axial resolution of the instrument with their anterior optics hack?

We estimated the pixel dimensions in our scanfield by correlating in vivo imaged regions with confocal images of the same areas in fixed retinal wholemounts. We have further corroborated the scale of our *in vivo* images by injecting 1 and 2 μm diameter microspheres into the retina and imaging these *in vivo*. The axial resolution is quite variable dependent on if the imaging field is in the center or peripheral region of the lens, as this greatly affects parallax. Unfortunately, microspheres injected into the vitreous are not stationary, thus we were not able to estimate axial resolution. This information has been added to our manuscript as Figure 7, which describes our imaging dimensions.

Page 16, line 579: Remove "designed for imaging other regions of the central nervous system"

This suggestion has been amended in the manuscript.

Page 17, line 612 et sqq.: What about the limitation that the animal pupil acts as a field stop? See comment about beam clipping.

Pupil dilation is absolutely critical for *in vivo* imaging and the fact that we cannot image the entire range of the retina would indicate there are some limitations due to beam clipping. We believe the efforts presented above in Reviewer Figure 1 define these limitations.

Reviewer #2:
This manuscript describes a procedure for two-photon (2P) fluorescence imaging of the mouse retina in the intact, living eye. 2P imaging in situ is of considerable current interest for addressing questions pertaining to progressive retinal disease but has been challenging because of the eye's optic properties including refraction from cornea and lens. The procedure described here is straightforward and uses readily available technology. The provided images substantiate the method and give fair proof of principle, applied to neuronal, glia, and vascular imaging. I have the following requests for additional detail and recommendations.

We thank the reviewer for their positive assessment of our submission.

Line 92: cut the glass pipette using what? Please provide more detail - scalpel blade? Razor blade? Iris scissors?

We are using a razor blade to cut the glass pipette. This information has been added to the protocol.

Line 110: Common, apparent refinement of this procedure would be to use Proparacaine 1% ophthalmic solution. One drop in each eye suffices and suppresses all eye lid and corneal reflexes within several seconds. Consider including this at least as an alternative approach.

We appreciate this suggestion, and have added this as an alternative in the protocol.

Much of the methods description is highly system specific, for example, line 253 references 'PMT C', the laser is presumed to be Spectraphysics MaiTai. Try to make it more generally applicable by leaving these details out and focusing on the function. 'Start up ultrafast pulse laser and ensure mode-locking'. 'Configure fluorescence emission collection path to sample green (505-525nm) light using appropriate dichroic filter sets (for example: XX, YY, ZZ; Chroma, US) and a photomultiplier tube (Hamamatsu XXX)'.

Line 309: assume that all samples are important. Describe 'best practice' procedures, only.

These are a very good points, we have made the descriptions as generic as possible throughout.

Line 446: Instead of clicking the "X" button to close the main controls and shut down ScanImage, consider using of the built-in 'scim_exit' function by typing that in the MATLAB command window. This lets ScanImage stop and 'clean up' all running processes and close all program windows in an organized manner.

We attempted this on our system, but it did not function as described. We would appreciate more information about this command. We have also removed mention of ScanImage to eliminate commercial language from the protocol.

Reviewer #3:
Manuscript Summary:
In-vivo 2-photon imaging of mouse retina is a challenge. In the manuscript authors describe an experimental protocol, which should allow to perform this experiment. Unfortunately, experimental approach, protocol and manuscript itself are full of weakness. The only one modification from the standard two-photon imaging microscope is an exchanging of the objective, which is not properly use according to specification. Described imaging protocol is danger for potential user. Authors don't understand terms which they are using, and they have no idea about the data which they collect. This manuscript Is not presenting any scientific value in this form.

We disagree wholly with Reviewer 3’s assessment of our manuscript.

Major Concerns:
1. Title "Transpupillary multiphoton in vivo imaging of cellular cohorts in the mouse retina" is suggesting, that there will be presented in-vivo imaging on neural activity in retina, because for that the 2 or 3-photon imaging is in use in neuroscience. There are other, much better methods for a just acquiring static images of cells anatomy. Authors in discussion (lines 620-626) describe it. So, there is no sense to use a relatively hight-power, low resolution 2P imaging for anatomical tracking of retina cells.

We have updated the title to reflect 2-photon imaging

2. Authors mentioned in discussion that "The only added components are an unusually long working distance objective to allow for the optical relay of the mouse lens, and a planar coverslip with transparent gel to partially correct for the cornea". First, what they want to correct?

Below is an image of our setup without the eye gel and coverslip to correct for the properties of the cornea.

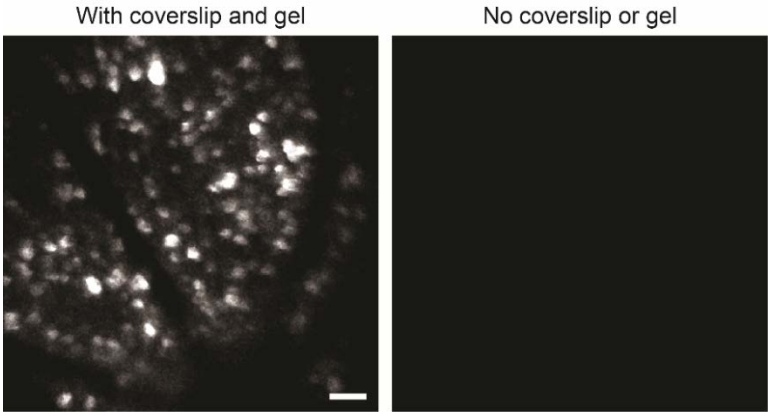

Reviewer Figure 3. Corrective components are required for imaging. *In vivo* fluorescence in RGCs was imaged as described with the methods in this manuscript (left). The same region was then imaged after removing the coverslip and gel from the eye and attempting to optimize z-position (right). Scale bar = 50 μm.

Second, according to the information form an incomplete list of materials, this objective is Mitutoyo WE715042319, from Edmund Optics (catalogue number 46-404). This is long working distance air objective, dedicated for cutting and trimming of semiconductor wafer and circuits (ideal for semiconductor and telecommunication inspection, or for laser cutting with common Nd:YAG lasers). And authors are using this objective, combine with coverslip, transparent gel and mouse eye. Authors probably never heard about refractive index mismatch, causing terrible distortion of excitation PSF (creating giant aberration). Combination of objective/air/coverslip/gel/eye optic patch is an excellent example of bad understanding principle of optics.

The aberration of the “air” objective mismatch through coverglass is trivial compared to the aberration caused by the mouse lens and cornea. Below is an image of 1 μm microspheres imaged through air and through our coverglass. There is little distortion cause by this mismatch.

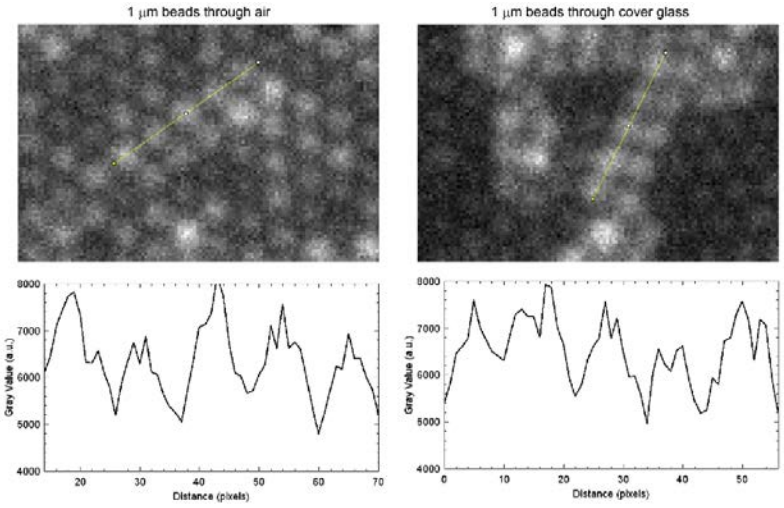

Reviewer Figure 4. Comparison of resolution imaging with and without coverglass. One micron diameter green fluorescent microspheres were air dried to a coverglass used in our protocol. The microspheres were then imaged with our 2-photon setup either through the air only (left) or through the coverglass (right) using the same scan settings. Pixel intensity histograms of the lines in each image are shown below.

Further, eye gel paired with either a contact lens or a coverglass imaged using an ‘air’ microscope objective is standard procedure for *in vivo* imaging of the mouse eye. Eye gel is required for imaging beyond 10-15 minutes to prevent the mouse cornea from desiccating, causing corneal opacity. We have described this aspect of the procedure in greater detail including a method to reliably position the coverslip in a fashion that we found significantly easier and more reproducible than more often reported contact lens application.

3. On experimental protocol, section 2: Microscope Setup, line 167, authors suggest pressing Enable button on the shutter controller as one of the first action, before turning on femtosecond laser and acquisition software. In each of the laser safety courses, the fundamental message is that the last mechanical shutter should be enabled only in a time of recording !!!!!!!! Behaviour presented by authors is extremely dangerous for the microscope users and other people in the same room. In a case of any problem with laser and microscopy hardware or software, this shutter is preventing user from a direct exposure of laser light, especially if as in this manuscript the eyepieces are in use, and there is a step for a hand exchange of filter cube.

We appreciate that Reviewer 3 has spotted this error and have adjusted the protocol accordingly.

4. Authors are trying to describe in detail all the steps on the microscope, but unfortunately only one information about this experimental setup is that it is a Hyperscope from Scientifica. This setup can be purchased with different configuration, so without schematic draw and info about principle components (scanning mirrors, PMTs, scan and tube lens, dichroic filters) it is extremely difficult to follow the guidance. This information should be included in a method paper.

We have added a schematic of our optical configuration to the manuscript as Figure 1.

5. I don't understand for what is a point 5: Measuring laser power. It is important to do this once when You install Your setup or make any modification on it, but not every day. If the authors have a problem with stability of the excitation power, I would recommend contacting with the service.

6. Authors in general are describing a lot of possible problems with this experimental setup (lines 181, 191, 198 and others). If this problem shows up on any setup, I will advise to contact with the service.

We wanted to provide a detailed description of measuring the laser power for the protocol. We have updated the manuscript accordingly.

7. In line 242 authors are mentioning abut possibility to PMT damage during cubes filter cubes changing and advise to do this in darkness. As a standard procedure, PMTs should be off for all the time when you are not recording, so I can't understand how it is possible that PMTs can be damaged? Are You trying to keep them on, with enabled shutter and modify optical patch in darkness?

As described in the protocol, the PMTs are off during filter changes. It is best practice not to expose PMTs to room light even without power across them.

8. Line 365. "obtain a flat imaging area", "retina is not flat with respect to the imaging light patch". Retina is lot flat due to the anatomy.In 2-photon microscopy shape of imaging area is related with a shape of excitation patch. I don't know how it looks like on this setup. according to a not standard objective and terrible distortion of the excitation PSF. In the method paper, author should present example of the image, which they want to obtain by adjusting "z-position of the stage until the fluorescence cells or structures in the retina come into focus".

We trust that a researcher can determine if their sample is in optimal focus.

9. Authors are collecting z-stack of images, and to create volumetric display of image data they use a maximum intensity projection function. It makes no sense. 2-photon microscopy operate on spatially limited excitation spot. Main advantage of this method is to acquire data from a tiny z-plane. In the authors approach, what will happen if there will be z-spatial overload of the two or more cells? Collecting of a 2-photon data z-stack allow to create a 3D reconstruction of cell anatomy (of course if the z-step is selected correctly), and this should be presentation of this data.

We use the maximum intensity projection function for display purposes. We have clarified this in the manuscript.

10. Line 486: "it may be beneficial to visualize changes to the image over time". I think that it will be beneficial to the authors if they will understand that 2-photon imaging microscopy is dedicated for that.
11. Line 617: "An alternative approach to correct this at the system level is adaptive optics which allows for subcellular resolution in the retina". An alternative approach to correct aberration will be using proper objective to create diffraction limited spot.

We have found that in order to image through the mouse pupil *in vivo* requires a microscope objective with a working distance of at least 10 to 10.5 mm. If Reviewer 3 could present a microscope objective that has such a working range, allows for 2-photon excitation wavelengths and emission collection of visible light, and has a higher numerical aperture than the one we describe in our set-up, we would be grateful for this information.

Minor Concerns:
1. Title "Transpupillary multiphoton in vivo imaging of cellular cohorts in the mouse retina" Authors are using 2-photon imaging, which of course is a kind of multiphoton imaging, but this term is suggesting that authors are trying to use 3-photon excitation for the experiment.

We have adjusted the title to indicate 2-photon imaging.

2. Line 106 - what is the max speed of centrifuging?

We have included the centrifugation speed.

3. Items described in lines 165, 166, 167 and other should have specify model name, not only producer.

We have added specifics for these items.

4. Line 198 - which version of ScanImage (not scanimage) ate You using?

We have added the ScanImage version to the Materials List.

5. All the safety warnings, line the one from line 206, should go to the beginning of procedure description.

We have moved and enhanced the safety warnings to the front of the procedure.

6. Line 252 - what is a "single wavelength emission imaging"? Are the authors measuring laser emission? Using a monochromator? Spectrometer?

This section has been removed from the protocol.

7. Line 362 - how authors are checking if the sample fluorescence is insufficient bright? Is there any scale for that?

Sufficient brightness at this step is subjective and used only for locating the target area to be imaged. We have added a description of when it may be beneficial to increase LED stimulation power.

8. Line 286 - authors are not describing how they operate on the change of z-dimension during imaging. Is this a piezo, hand or motored moved engine?

We have added the motorized objective to the microscope description.

9. Line 547 - I am not sure of what You are creating, but it is not a lens, it is a just an immersion of gel.

Any non-light absorbing liquid that is not flat at the point of light entry and/or exit will create a lens.

10. Line 557 - there are no scale bar on Fig. 2.
11. Line 562 - the same as above.

We have added scale bars to all figures.

12. Line 580 - 20 mm is not an unusual working distance for air objective.

It is for a relatively high NA objective. We tested using ‘standard’ air objectives, which typically have an NA of at best 0.25 and were not able to image on our setup. We have added this information to the manuscript.

13. Line 582 - correct of what?

We have clarified this in the text.

14. Line 583 - Based on what authors claim that ACs and RGCs are the main neuronal components of the retina?

We have clarified this in the text.

15. Line 612 - a limitation of this approach is the fact that aberrations are created, not corrected.

The aberrations inherent to the cornea and lens are far greater than any issues caused by coverglass or eye gel.

16. Line 616 - what is the out of focus light in 2P excitation?

We have clarified this in the text.

17. There is no info about field of view in this configuration.

We have measured the range of imaged area in a single orientation and the data is presented below. We can image an area of roughly 650 μm^2 in a single orientation. If we tilt the angle of the head across a single rotational axis, we can access a linear range of 2.2 mm, and thus estimate an area of the retina across 3.8 mm^2 is accessible for in vivo imaging with our setup (See Reviewer Figure 1). We have added this information to the text.

18. List of materials should be upgraded on all of the 2-photon setup important elements (acquisition software, PMTs, scanning mirrors etc.)

We have added these components to the list of components/reagents.

Reviewer #4:
Manuscript Summary:
In the manuscript entitled "Transpupillary multiphoton in vivo imaging of cellular cohorts in the mouse retina", Wang et al. presented a protocol of using standard two-photon microscope for in vivo imaging of mouse retina. The current form of the manuscript needs a major revision to be acceptable for the publication in JoVE.

Major Concerns:
#1: The reported protocol proposed minor adaptations to a commercial two-photon microscope system for in vivo retinal imaging. However, it ignored the fact that the imaging quality in terms of resolution and fluorescence intensity are inevitably degraded by the optical aberration of mouse eye. Therefore, a major question that must be clearly addressed is what exactly can be interpreted from the low-resolution images acquired by the two-photon imaging system. For example, the authors claimed that fluorescence intensity of cell soma can be easily quantified (5th paragraph in the discussion section). However, the fluorescence intensity are significantly affected by the mouse eye aberration which could vary from animal to animal or measurement time to time. The effect can be seen in Figure 2 that although the same imaging site can be relocated in time-lapse imaging based on the vascular landmarks, the fluorescence intensity and distribution of retinal ganglion cells between the two imaging sessions are largely different (especially the bottom row of Figure 2). Without correction of the aberration, the quantification of fluorescence intensity of cells is not reliable. In the revised manuscript, I would suggest the authors focus on cell counting that does not require high imaging resolution. The authors could demonstrate a detailed procedure of in vivo RGC or other neurons counting using an image processing tool, such as Fiji.

We agree with the reviewer and have updated our manuscript accordingly. While we do believe intensity based measurements can be applied to acute experiments where head position is maintained constant across images, in samples that are examined chronically, assessments relying on ratiometric read outs are far more reliable in this system.

#2: As correctly pointed out by the authors, one major advantage for two-photon retinal imaging is to use NIR laser that can avoid stimulation of intrinsic visual response of retinal neurons. Since the authors used a calcium sensor, Twitch2b, for visualization of retinal ganglion cells and amacrine cells, it would be of great interest that the authors can demonstrate the functional calcium imaging capability apart from structural imaging.

We have investigated calcium responses in RGCs in our preparation using the FRET ratiometric sensor Twitch2b. Similar to previous reports from retinal explants, we have found that onset of laser scanning induces a calcium increase in RGCs that returns to baseline in most neurons (see Figure 8). We attempted to add UV LED stimulation to our microscope setup, but unfortunately we were not able to procure the custom mirrors needed to adapt our light path in the time frame for these revisions. However, the 2-photon power that we use for scanning is within the range of previous reports that have observed light responses, and we can clearly observe transient changes in activity in RGCs. Thus we believe it would be entirely feasible to image circuit activity with our approach. This information has been added to the manuscript.

#3: For the microglia imaging, one of the most important goal is to examine the inflammatory activity in the retina by direct visualizing the typical amoeboid morphology of reactive microglia. In Figure 4, however, the detailed morphology of most microglia in the field of view were not clear. This prevents rigorous judgment on microglia states and thus is unable to identify inflammatory activity at an early stage of eye diseases. The limitation, again due to poor resolution, should be pointed out and discussed in the manuscript.

To address this point, we have performed excitotoxic lesions of the retina by injecting NMDA intravitreally in CX3CR1-GFP transgenic mice. In line with the literature, we see microglia with amoeboid morphology as compared to untreated retinae. This data has been added to the manuscript.

#4: In line 230, the authors stated that maximal laser power without causing photodamage to the retina is ~50mW in their two-photon imaging system. However, the microscope system used by others could be different. I would suggest the authors to work out a general procedure or criterion to determine the laser power threshold of a microscope with different optical configuration for safe retinal imaging.

We have further characterized the damage (or lack thereof) caused by our *in vivo* imaging setup and present this data above in Reviewer Figure 2. This information has also been added to the manuscript. Additionally, we have added a section to the discussion describing strategies for laser tolerance.

5: In line 435, as pointed out by the authors, the clarity of mouse eye is crucial for high-quality retinal imaging. How did they quickly identify whether the mouse eye is still in good and transparent condition during a continuous imaging experiment? How to restore the clarity of a drying or opaque eye?

Development of cataracts cannot be restored and is usually caused by improper intravitreal injection. Corneal drying will often occur if the non-imaged eye is not properly maintained. We have added a method to maintain the non-imaged eye during experiments. Corneal opacity due to desiccation can resolve on its own over the course of a few days. We have added this information to the manuscript.

Minor Concerns:
#6: In the 3rd paragraph of the discussion section, the CAG promoter has not been used in the experiments.

We have edited this accordingly.

#7: The calibration of scale bar of the retinal images should be also discussed in the protocol.

We estimated the pixel dimensions in our scanfield by correlating in vivo imaged regions with confocal images of the same areas in fixed retinal wholemounts. We have further corroborated the scale of our *in vivo* images by injecting 1 and 2 μm diameter microspheres into the retina and imaging these *in vivo*. This information has been added to our manuscript as Figure 7, which describes our imaging dimensions.

#8: In line 252, a 605/70 band pass filter was used for the collection of Evans Blue signal. In fact, the emission peak of Evans blue is ~680nm. Why wasn't a band pass filter centered at 680 nm used?

This was an error on our part, we have updated the description of the optical components to image Evans Blue.

#9: To minimize the stress of mice, a contact lens would be a better choice. The authors simply placed a coverslip on the eye which would introduce extra pressure to the mouse eye and more importantly increase the eye aberration.

In our initial experiments, we tested the use of a contact lens and found it much more challenging to work with because it is not stable and extremely difficult to orient perpendicular to the microscope objective. It is important to note that the coverslip does not touch the mouse eye. It is maintained in a microscope holder at a small distance above the cornea. This should cause less stress to the eye since a contact lens would rest on the cornea. We have updated our description to make this clear including adding panels to Figure 2, and added comparisons with contact lens imaging to the Discussion.